*Available online www.jocpr.com*

**Journal of Chemical and Pharmaceutical Research, 2017, 9(3):141-152**

**Research Article**

**ISSN : 0975-7384**
**CODEN(USA) : JCPRC5**

# Study of the Corrosion-Erosion Behavior of Cu70-Ni30 Alloy Inflowing Water Containing Marble Particles

**Laidi Babouri[1], Kamel Belmokre[2], Smail Brioua[2] and Jean-François Bardeau[3*]**

*[1]School of Higher Education in Skikda, Algeria*
*[2]Department of Materials Science, University of Skikda, Algeria*
*[3]LUNAM University, IMMM, UMR CNRS 6283, Avenue Olivier Messiaen, 72085 Le Mans Cedex 9, France*

---

**ABSTRACT**

*This paper reports on the study of copper-nickel alloy (Cu70-Ni30) surface modifications during the corrosion-erosion process taking place in flowing water containing marble particles. The surface modifications were evaluated at room temperature under agitation by potentiodynamic polarization curves and Electrochemical Impedance Spectroscopy (EIS). The electrochemical measurements showed that the corrosion current density decrease from 6,3mA/cm$^2$to 4,8 mA/cm$^2$ whenthe marble powder concentration increases from 0 to 8 ppm. The morphology and the nature of corrosion products, formed on the copper alloy surface, were studied by optical microscopy and micro-Raman spectroscopy. At low concentration (from 0 to 4 ppm) the structural analysis showed the presence of $Cu_2O$ and CuO compounds while at 8 ppm the passive films are formed of $Cu_2O$ and NiO. White deposits of $CaCO_3$ and a local abrasion are also evidenced for 8 ppm. The mechanism of Cu70-Ni30 corrosion-erosion as function of marble powder concentration are discussed. At low concentration (2 and 4 ppm) the presence of marble solid particles in flowing water leads to erosion and corrosion of the surface and for 8 ppm both erosion and abrasion are clearly observed.*

**Keywords:** Marble particles; Copper-Nickel alloy; Erosion; Abrasion; Electrochemistry

---

## INTRODUCTION

Marble is one of the particularly precious stones [1]. Indeed, this metamorphic stone composed of calcite ($CaCO_3$) is extremely hard. It was formed with recrystallization of ancient limestone and dolomite under intense pressure and heat during geologic processes [1-4]. Regarding its mechanical and chemical resistance, marble presents same technical characteristics as limestone. The compressive strength is between 70 and 150 N/mm², and porosity is rarely greater than 1.5 % [5]. Because of its remarkable physical and mechanical properties (density, brightness, porosity, crushing strength, abrasion resistance), marble is used as a building material and outdoor sculpture as well as for sculpture bases. In architecture, it is also used in exterior walls and veneers, flooring, decorative features, stairways and walkways [6].

The high-quality finished products of marble are obtained by the transformation of raw blocks extracted from quarries. The transformation cycle follows a fairly simple technological process based primarily on the sawing operation. During the cutting process, around 25% of the original marble mass is lost as dust [7]. The industries use diamond tools for cutting and sawing marble. This is an effective technic when used with a water irrigation system. The presence of water ensures both lubrication of the tool and evacuation of generated cutting dust.

The wastewater is then evacuated through copper alloy pipes, especially Cu-Ni alloys [8,9] because such alloys are mainly recommended for its excellent resistance to corrosion in aggressive environments. Indeed, they have shown an excellent behaviour in seawater against biofouling [10] due to their electrochemical properties and the formation of oxide and/or hydroxide compounds covering the metal surface [11,12]. It has been reported that cuprous oxide $Cu_2O$, cupric oxide CuO and copper hydroxychloride $Cu_2(OH)_3Cl$ are the predominant passive elements [13,14] formed in aqueous medium.

The incorporation of nickel in the alloy allows the formation of compounds such as $Cu_3Ni(OH)_6Cl_2$ and NiO [12]. Once again, the presence of aggressive environments can significantly modified the surface topography and the composition of such alloys [13-15]. Indeed, the presence sulfides and ammonia may expose them to different forms of corrosion such as localized corrosion [16-21], crevice corrosion [22-24] and selective corrosion [25-29]. If water contains carbonates, sulphates and phosphates suspension, it may give rise to the formation of tartar, which generates also corrosion and cracks. On the other hand, the presence of solid marble particles into turbulent flows can cause the erosion of the protective corrosion layer leading to increase the density of solid particles into the whole wastewater supply network. Such phenomenon is known to be the main reason for malfunction, failures in hydraulic systems.

Consequently, the corrosion resistance of copper nickel alloys depends upon formation of a strong protective film. Film formation is affected by pH, time, aeration, velocity, temperature, pollution and other factors. There is generally an inner cuprous oxide film, $Cu_2O$, and an outer cupric oxide film, CuO [30,31].

The impingement of solid particles, entrained in a flowing liquid, can damage both types of protectives films (thick diffusion barriers and thin passive film) leading to erosion-corrosion and resulting in more exposure of the metal to corrosion. The particles may also erode the metal [32].

So, the aim of this work is to better understand the behaviour of copper-nickel pipes and specially the Cu70-Ni30 alloy used in irrigation water supply circuit when marble particles are present. Our study will focus on the physical and chemical behaviour of the interface of the Cu70-Ni30 alloy in tap water containing marble powder. The chemical composition of the layer was studied by Energy Dispersive Spectroscopy (EDX) and micro-Raman spectroscopy. Electrochemical investigations have been carried out using stationary and transient techniques to emphasize the kinetics and reaction mechanisms.

## EXPERIMENTAL SECTION

### Marble powder preparation

The white marble powder was obtained from the crushing blocks of marble extracted from Fil-Fila deposits, located at 25 Km east of Skikda city (Algeria). Note that, marble samples acquire a variety of colours due to the presence of some oxides and salts.

### Water preparation

The corrosion tests were conducted in both aerated and agitated tap water. The “muddy” water solution is obtained by adding the marble powder to the tap water in order to simulate the recycled industrial water. The concentrations of the marble powder in tap water retained for this study varies from 2 to 8 ppm. The choice of these concentrations results from a periodic analysis of the recycled water used in the cooling process and lubrication of marble cutting and polishing tools at the Skikda plant in Algeria.

### Samples preparation

The material used in this study is a Cu-Ni alloy, provided by the Skikda marble processing plant (Algeria) and made by SNC-Lavalin Group Inc (Canada). The cupronickel coupons used were cut into1.5 × 1.5 × 0.08cm.Before each test, the samples were polished with successive grades of SiC emery papers from 400 to 4000 grit numbers to achieve mirror finishing. The electrode was thoroughly washed with distilled water, degreased in acetone, rinsed with distilled water and dried under forced-air-drying. The whole procedure was followed before each electrochemical experiment. The quality of the sample preparation is important because it minimizes the presence of surface heterogeneities [33].

For the batch experiments, the samples were immersed in400 ml of aerated tap water in the absence and presence of marble powder under magnetic stirring bar at the bottom to 'simulate' a flowing water. Theaging time is 30 days at room temperature.

### Analysis

The chemical composition of the alloy was investigated by using an Energy Dispersive Spectroscopy (EDX) coupled to a Scanning Electron Microscope JEOL Model JSM-5800 LV. The analyses were carried out under an accelerating voltage of 15 kV. The Si(Li) detector was equipped with a thin beryllium window that allows detect and quantify the oxygen. Structural analysis of non-corroded alloy was achieved by using a Siemens D500 diffractometer in a Bragg- Brentano geometry using Cu-$K\alpha_1$ radiations ($\lambda_1$ = 1.54051) as X-ray source (cold cathode Crookes tube). The measurements were carried out in the $2\theta$ range 5-100° with a step size of 0.02° and a count time of 20s per step. The physical and chemical analysis of water was done using gravimetric techniques, volumetric and colorimetric. For dosing elements such as calcium, magnesium, copper, iron, we have used an atomic absorption AA-6800Shimadzuspectrometer, equipped with a hollow-cathode lamp and a nebulizer-burner assembly air-acetylene. The apparatus Multi 340i WTW brand allowed to obtain the pH, temperature, salinity and dissolved oxygen content (*DO*).

The identification of both the corrosion products and the structural phases formed on alloy surface were confirmed using Raman spectroscopy. Indeed, Raman spectroscopy is an effective tool to investigate the structure of corroded alloys and steels [12,34-36]. The measurements were carried out on the surface of cupronickel coupons corroded for 30 days at free potential. The Raman experiments were performed at room temperature using a T64000 Jobin-Yvon/Horiba spectrometer equipped with a 600 lines/mm diffraction grating and a nitrogen cooled CCD detector. The Raman spectra were recorded under a microscope (Olympus Bx41) in the backscattering geometry with a 100× objective focusing the 514 nm line from an Argon–Krypton ion laser (Coherent, Innova*).* The spot size of the laser was estimated at 0.8µm and the spectral resolution at 2 $cm^{-1}$. The Raman spectra were recorded using low laser output powers between 1 and4mWin the wave number 80-2000 $cm^{-1}$ region with an integration time of 400 s. Acquisition and basic treatments of spectra have been made with the LabSpec V5.25 (JobinYvon-Horiba) software.

The average surface roughness (*Ra*) was determined by using Mitutoyo'sSJ-301Surftest surface roughness tester within sampling length 2.5 mm. The surface morphology of Cu-Ni surface alloy was observed by an Olympus BXFM-F optical microscope. The electrochemical studies were carried out using Potentiostat/Galvanostat model PGZ 301, Radiometer Analytical using a three electrodes cell with a platinum electrode as counter electrode ($C_E$), saturated calomel electrode (SCE) as reference electrode ($R_E$) and the samples of cupronickel with an exposed surface area of 1 $cm^2$as working electrode.

Polarization curves were obtained in a scanning field (-900 to 800) mV/(Ag/AgCl). The potential was incremented by scan rate of 0.5 $mV.s^{-1}$. This rate scan allowed us to be in quasi-stationary conditions (necessary for good reproducibility results) [12]. All curves were corrected for ohmic drop previously determined by electrochemical impedance spectroscopy (EIS).

Electrochemical impedance measurements were completed in the frequency range from 100 kHz -10 mHz with sinusoidal wave amplitude of 10 mV.

Corrosion parameters were extracted from polarisation and EIS plots. Polarisation curves were analysed using VoltaMaster 4 software by Tafel extrapolation (linear parts of anodic and cathodic branches) technique. The spectra of EIS were modeled with an equivalent circuit proposing with **"**Zview 6.0" software according to the electrochemical phenomena. All of the electrochemical Data were recorded after a period of 1 h (for stabilizing conditions).

## RESULTS AND DISCUSSION

### Structural analysis

The chemical composition of non-corroded Cu-Ni alloy, determined by Energy Dispersive Spectroscopy (EDX) is given in Table 1. Figure 1 shows (XRD) patterns of the copper alloy. The diffraction peaks are indexed to cubic crystal structure with space group *Fm-3m* (JCPDS Card N°: 03-065-7246). The crystallographic analysis shows unambiguously the characteristic lines of the $\alpha$-phase for the Cu-Ni alloy [12]. Indeed, when a copper content is higher than 63 %,Cu-Ni alloy has single phased microstructure [37]. The $\alpha$-phase structure is characterized by a high ductility and a good impact resistance even at temperatures below the freezing point.

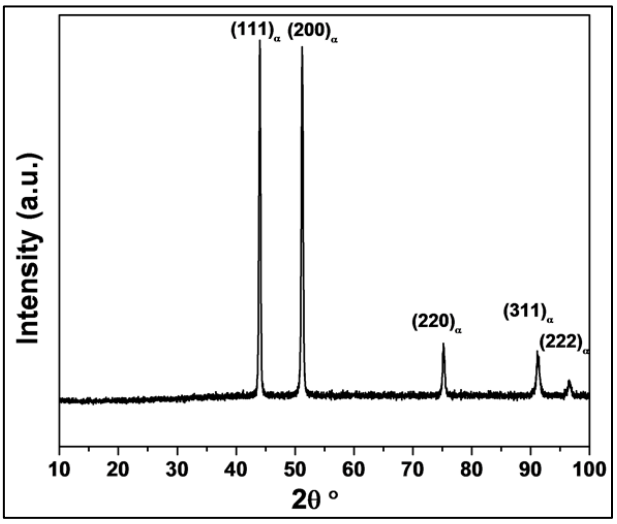


**Figure 1: X-ray diffractogram of the Cu-Ni alloy**

**Table 1.Elemental chemical composition of Cu-Ni alloy (in atomic %)**

| Alloys | Elements | | | | |
|---|---|---|---|---|---|
| Composition (%) | Cu | Ni | Al | Fe | Mn |
| | 66 | 30.4 | 2.6 | <1 | <1 |

The physical and chemical characteristics of tap water used in this study are presented in Table 2.The quality of the water revealed that it contains many dissolved ions. The main ions are calcium ($Ca^{2+}$), magnesium ($Mg^{2+}$) and chloride ($Cl^-$). Less concentrated, water also contains nutrients, such as nitrogen (contained in ammonia, nitrates) and phosphorus (contained in phosphates). Other elements are present only in trace quantities, such as copper and iron. Finally, the silica content is about 1.74 mg/l and the content of dissolved oxygen is relatively low. Therefore, regarding the values of the Table 2, the contents are well below the standards set by the World Health Organization.

**Table 2.Physical and chemical characteristics of the tap water**

| Parameters | Content |
|---|---|
| pH | 7.3 |
| Ca (mg/l) | 14 |
| $Mg^{++}$ (mg/l) | 3.1 |
| $Cl^-$ (mg/l) | 96.5 |
| $Fe^{+++}$ (mg/l) | <0.02 |
| $Cu^{++}$ (mg/l) | <0.02 |
| $SiO_2$ (mg/l) | 1.74 |
| R-$Cl_2$ (mg/l) | 1.2 |
| $NH_4^+$ (mg/l) | 0.9 |
| $NO_3^-$ (mg/l) | 2 |
| $PO_4^{---}$ (mg/l) | 0.4 |
| Dissolved oxygen (mg/l) | 8.4 |

The physicochemical and mineralogical characteristics of the marble used are summarized in Tables 3and 4.

**Table 3.The physical characteristics of marble**

| Characteristics | Petrographic | Color | Density (Kg/m3) | Specific surface ($cm^2/g$) |
|---|---|---|---|---|
| Powder < 80µm | Microcrystalline limestone | White | 650 | 3448 |

**Table 4.Chemical composition of the marble powder**

| Oxides | $CaCO_3$ | MgO | $SiO_2$ | $Al_2O_3$ | $Fe_2O_3$ |
|---|---|---|---|---|---|
| Composition (% by mass) | 98 | 1.96 | 0.73 | 0.23 | 0.15 |

In Figure 2, the Raman spectrum of the white marble are characterized by four vibrational bands: the low frequency lattice modes at 154 and 281 $cm^{-1}$ are clearly visible with the weak band at 711 $cm^{-1}$ and a strong internal mode of carbonate at 1085 $cm^{-1}$of $CaCO_3$ crystallized in the calcite structure [37,38].

It is evident that the principal ingredient of the marble is $CaCO_3$. Nevertheless, different mineral grains with black dots were also observed (Figure 2-a point 2). Raman investigations identified the mineral grains as dolomite ($(Ca,Mg)(CO_3)_2$, Figure 2-c) [39,40]. These black minerals are interpreted as secondary minerals formed by the dolomitisation of the original limestone and these inclusions are trapped in the crystals during what is called the dolomitisation.

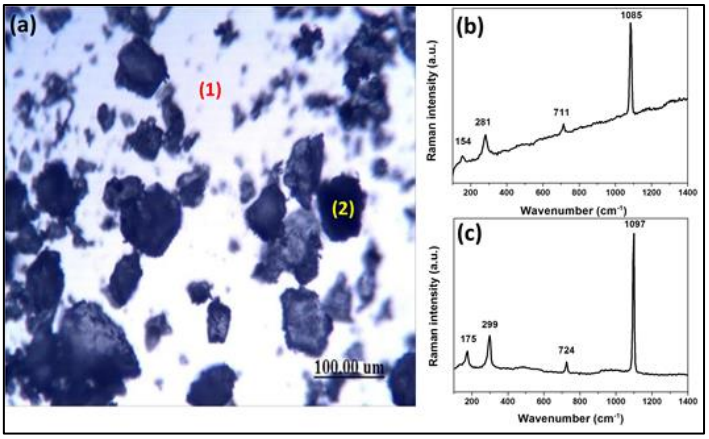


**Figure 2: (a) Optical microscope image of marble powder; (b) Raman spectrum of $CaCO_3$ 'point 1'; (c) Raman spectrum of dolomite ($CaMg(CO_3)_2$) 'point 2'**

Because of their unique vibrational spectrum and distinguishable peaks, minerals and inorganic compounds are easily identifiable from their Raman spectra. That's for this reason that Raman spectroscopy has been widely

used as an analytical tool for the identification of materials in particular when minerals have the same functional group (i.e. $CaCO_3$). In that case, by observing the low-frequency lattice modes, it becomes quite easy to distinguished between calcite, aragonite, vaterite, dolomite ($CaMg(CO_3)_2$), magnesite ($MgCO_3$) [38,41]. So, the spectrum of the black grains was recorded in the 100-1400 $cm^{-1}$ region with good ratio signal to noise (Fig. 2). The low frequency lattice modes at 175 and 299 $cm^{-1}$ are characteristic modes of the dolomite lattice hat is moreover confirmed by the presence of bands at 724 and 1097 $cm^{-1}$ attributed to bending and stretching mode of carbonate ions respectively [39]. Batch experiments were conducted for 30 days in tap water in the absence and presence of 8ppm of marble powder. After 30 days of immersion at free corrosion potential, the alloy surfaces were analysed both by optical microscopy and Raman spectroscopy.

Optical images of the surface of the Cu-Ni alloy are shown in Figure 3.

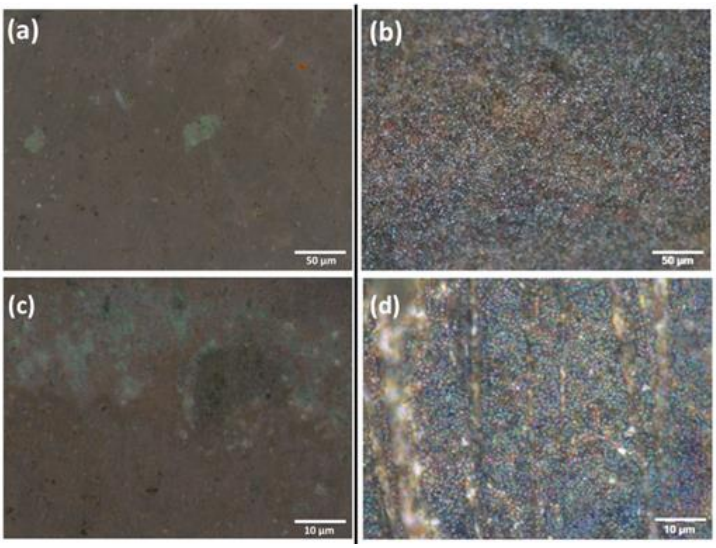


**Figure3: Optical microscope images of the surface of the Cu-Ni alloy corroded in; (a) tap water in the absence of the marble powder; (b) in the presence of 8 ppm of marble powder**

In the absence of marble, the images revealed the formation of a greenish oxide layer. The surface of the cupronickel alloy in the presence of 8 ppm of marble powder shows a local abrasion compared to that in absence. In the presence of marble powder, the analysis of the alloy surface shows the presence of white deposits, which confirms the precipitation of calcium carbonate.

The roughness (*Ra*) of Cu-Ni surface in the absence of marble powder is 0.03µm, while in the presence of 8 ppm of marble powder in water the *Ra* of the sample surface rises to 1.3µm. We attribute this difference to abrasive solid marble particles entrained in water, which impinge on the Cu-Ni alloy surface and cause the removal of the protective oxide film.

Figure4 shows the Raman spectra of the corrosion products formed on the Cu-Ni alloy surface immersed in tap water in the presence and absence of marble powder. The Raman spectra of the cupronickel surface in the absence of marble powder show the characteristic phonon frequencies of the crystalline of CuO and $Cu_2O$.$Cu_2O$ belongs to $O_h^4$ space group with simple cubic lattice and two formula units per unit cell [42]. According to group theoretical calculations, it has six zone-center optical phonon modes [43], which are represented as: $\Gamma = F_{2g} + 2F_{1u} + F_{2u} + E_u + A_{2u}$. The $F_{2g}$vibrational mode is Raman-active and the two $F_{1u}$modes are IR active for a perfect $Cu_2O$ crystal. However, the defects present (including oxygen and copper site defects) in a crystal lattice may activate the silent modes, and for this reason additional bands can be observed in the Raman spectrum of $Cu_2O$ [43-46].

Figure 4 shows the Raman spectrum for $Cu_2O$, with four distinct bands located at 155, 220, 415 and 630 $cm^{-1}$ respectively. The observed Raman bands are assigned as follows: Raman allowed mode $F_{2g}$ at 520 $cm^{-1}$ [44], two IR active modes $F_{1u}$at 155 and 630$cm^{-1}$ [45] and overtone $2E_u$at 220 $cm^{-1}$[46]. The mode at 415 $cm^{-1}$is generated by a multi-phonon process [44]. In addition, the weak peaks observed at 315, 525 and 730 $cm^{-1}$ are commonly assigned to the second-order modes of $Cu_2O$ [43-46]. CuO has monoclinic symmetry with space group *C2/c* [47,48]. CuO has 12 phonon branches. A factor-group analysis gives the following zone-center modes: $\Gamma = A_g + 2B_g + 4A_u + 5B_u$. The three acoustic modes are of $A_u + 2B_u$ symmetry. Among the nine optical modes, three ($A_g + 2B_g$) are Raman-active, and the remaining six modes ($3A_u + 3B_u$) are IR-active [49]. The Raman spectrum with intense peak at 298$cm^{-1}$ and less intense at 345 and 628 $cm^{-1}$can be attributed to the three Raman active modes expected for CuO [50]. The peak at 298 $cm^{-1}$is assigned to $A_g$ mode whereas the two latter peaks are assigned to $B_g$ modes of CuO, respectively.

In the presence of marble powder, our investigations show similar spectra for $Cu_2O$ and on the surface Raman measurements reveal additional vibration modes of assigned to $CaCO_3$ and NiO [51,52]. In alkaline waters, it

has been suggested that copper (II) hydroxide ($Cu(OH)_2$) is the initial corrosion product formed. The copper (II) species is then transformed into the much less soluble copper oxides ($Cu_2O$ and CuO). Regarding the medium and in particular the presence of carbonate of calcium, it is not surprising to find traces of such material onto the surface. Such a result is nevertheless important because the presence of these minerals contribute to limit the dissolution of copper and then reduce the corrosion process of Cu-Ni alloy [53].

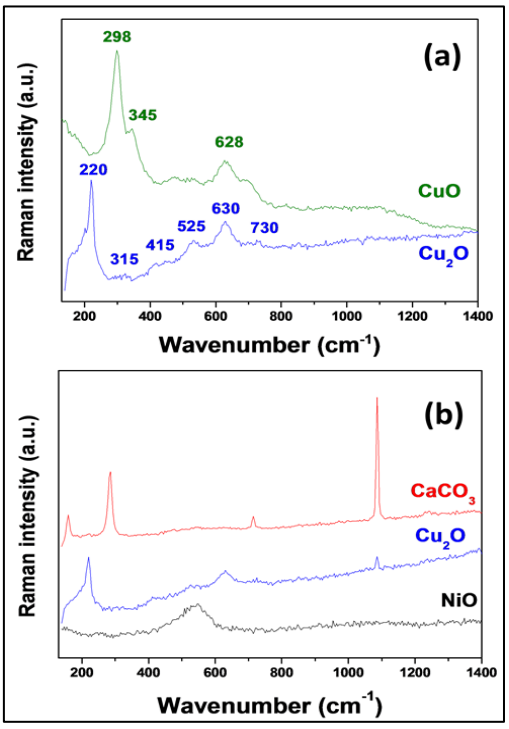


**Figure 4: Raman spectra of the corrosion products formed on the cupronickel surface after 30 days in tap water(a) in the absence of marble powder,(b) in the presence of 8 ppm of marble powder**

The corrosion rate was determined according to the ASTM standard method for corrosion measurement; the corrosion layer was pickled with HCl (15%) and isopropanol with 5 mg/l of hexamethylenetetramine to inhibit further corrosion.

The corrosion rate can be calculated using the following formula [36]:

$$\text{Corrosion rate (micron/year)}: \frac{3650 \text{ x weight loss (mg)}}{\text{Density (g/cm}^3\text{) x Area (cm}^2\text{) x Time (days)}} \quad \text{(Eq.1)}$$

With a density of 8.9 g/cm$^3$ for cupronickel.

The corrosion rates calculated from weight loss after 30 days of immersion in tap water are 21.6 µm/year in the absence of marble powder and 33.2 µm/year in the presence of marble. This result showed that the presence of marble powder increases the corrosion rate of cupronickel due to the phenomenon of erosion.

**Electrochemical analysis**

In order to understand the phenomenon taking place at the interface with the metal, we have undertaken the study of the electrochemical behaviour of the Cu-Ni alloy by stationary and transient electrochemical methods

The free corrosion potentials of cupronickel (Cu70-Ni30) in tap water, in the absence and presence of different concentration of marble powder, are presented in Figure 5.

We can distinguish in Figure 5the appearance of two zones. The first zone (Zone I) appears from 0 to 10 min. In this zone a decrease in potential is observed, attributed to continuous attack of alloy. The second zone (Zone II) that begins beyond 10 minutes is characteristic of fluctuation of the potential until to a relative stability resulting from the total polarization of the surface of the alloy.

The thermodynamic equilibrium potential is assumed to be of the same order of magnitude for the different concentrations of the marble powder. In Figure 5, the potentials stabilized at a quasi-stationary value around -130 ± 10 mV/(Ag/AgCl). When the alloy Cu70-Ni30 is in contact with the solution containing 2 and 4 ppm, the behaviour is mainly governed by the hydrodynamic effect. Indeed, the solubility of the solution is not involved since the calculation of the solubility product ($K_S$) for both concentrations show that log($K_s$) values are greater (Table 5) than 8.42 [54] (determined for the equation 2).

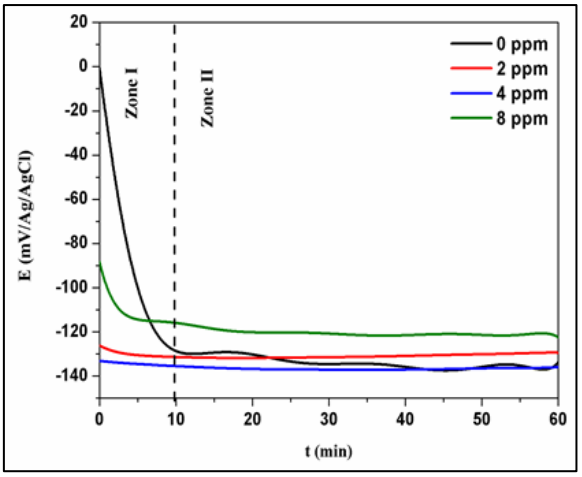


**Figure 5: Evolution of the free potential of the Cu-Ni alloy recorded in tap water, in the absence and presence of different concentrations of marble powder**

For 8 ppm, log($K_S$) is equal to 8.2 favouring the precipitation of the calcite ($CaCO_3$) (**Eq.2**) onto the metal surface with a high coverage rates.

Given that, the main chemical constituent marble powder is calcite ($CaCO_3$).Its dissolution equation is:

$$CaCO_3 \rightleftarrows Ca^{2+} + {CO_3}^{2-} \text{ with } \log(K_s) = 8.42 \text{ at } 25°C \quad \text{(Eq.2)}$$

The values of $K_s$ corresponding to different concentrations of marble powder are given in **Table 5**.

**Table 5: $K_S$ values as function of the concentration of the marble powder**

| Marble powder concentration (ppm) | $Ca^{Z+}$ Mol/l | $Co_3^{Z-}$Mol/l | log($K_s$) |
|---|---|---|---|
| 2 | $2.10^{-5}$ | $2.10^{-5}$ | 9.4 |
| 4 | $4.10^{-5}$ | $4.10^{-5}$ | 8.8 |
| 8 | $8.10^{-5}$ | $8.10^{-5}$ | 8.2 |

The results of the potentiodynamic polarisation curves study of Cu-Ni in tap water in the absence and presence of marble powder as function of concentrations are shown in Figure 6. The corresponding electrochemical parameters are summarized in Table 6.

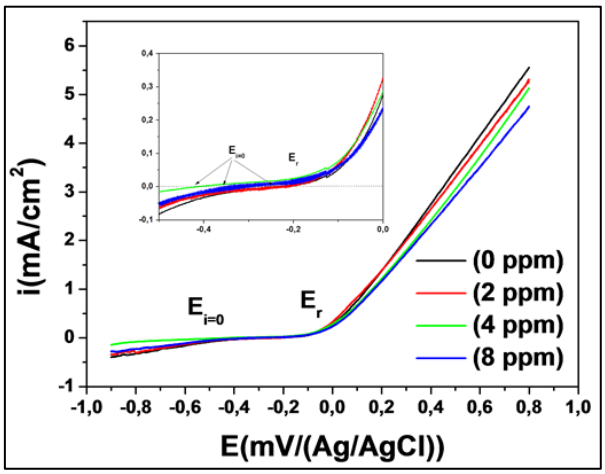


**Figure 6: Polarization curves of the Cu-Ni alloy in tap water, in the absence and presence of marble powder with different concentrations of marble powder**

The analysis of the polarization curves shows that the cathodic branch, which extends from the starting potential to the corrosion potential ($E_{i=0}$), is characterized by a relatively well-defined current plateau attributed [46] to the reduction of the oxygen dissolved in the solution between the electrodes:

$$\frac{1}{2}O_2 + H_2O + 2e^- \rightarrow 2OH^- \text{ (Eq.3)}$$

On the anodic branch of the polarization curve, two areas can be distinguished. The first area is observed between $E_{i=0}$ and $E_r$, where the corrosion current density is almost zero. This phenomenon could be attributed to the formation of a film composed by adsorbed species, such as copper oxide and nickel oxide. Copper oxide layers consist either of a simple oxide layer cuprite ($Cu_2O$) or a mixed layer of cuprite and tenorite (CuO), which can result from the oxidation of cuprite.

The second area above $E_r$ is characterized by a sudden rise in current density. This phenomenon is likely due to a rupture of the passive film previously formed. This rupture makes the metal surface directly exposed to the electrolyte and leading to migration of metallic ions into the solution [12]. The analysis of electrochemical parameters (**Table 6**) revealed that the addition of the marble powder on tap water increases the corrosion potential ($E_{i=0}$), while lowering corrosion current densities.

**Table 6: Electrochemical parameters of the Cu-Ni in tap water in the absence and presence of marble powder**

| Marble concentration (ppm) | *E*i=0 (mV/(Ag/AgCl) | $E_r$ (mV/(Ag/AgCl) | $I_{i=0}$ (mA/cm$^2$) |
|---|---|---|---|
| 0 | -424 | -63 | 6.3 |
| 2 | -233 | -56 | 5.6 |
| 4 | -233 | -55 | 5.4 |
| 8 | -315 | -42 | 4.8 |

In the anodic zone, usually the reaction mechanism of dissolution of the Cu-Ni alloy in an aqueous medium follows successive steps:

First, the dissolution of the copper alloy according to the following reaction [12]:

$$2Cu \longrightarrow 2Cu^{+} + 2e^{-} \text{(Eq.4)}$$

After, the ions ($OH^-$) released from the reduction of water and in the presence of metal ions, contribute to the formation of copper oxide, according to the reactions (Eq.5and Eq.7)

$$2Cu^{+} + H_2O \rightarrow Cu_2O + 2H^{+} \text{(Eq.5)}$$

$Cu^+$ cations (which are available at the metal/cuprite interface), after migrating through the layer cuprite ($Cu_2O$), can further form cuprite and thus increase the thickness of the passive layering contact with the corrosive medium, or give $Cu^{2+}$ ions according to the following reaction:

$$Cu^{+} \longrightarrow Cu^{2+} + e^{-} \text{(Eq.6)}$$

The diffusion of ions through the cuprite layer is the step that slows the corrosion phenomenon. This oxide film can be described as passive film. Cuprite layer can then be oxidized to tenorite, CuO, in contact with the corrosive medium [55-47], as described by the following equation:

$$Cu_2O + H_2O \rightarrow CuO + 2H^{+} + 2e^{-} \text{(Eq.7)}$$

Part of the cuprite layer may also dissolve[58],according to the reaction:

$$Cu_2O + 2H^{+} \rightarrow 2Cu^{+} + H_2O + 2e^{-} \text{(Eq.8)}$$

The ions ($OH^-$) released from the reduction of water (Eq.3) in the presence of metal ions contribute to the formation of nickel oxide, according to the following reactions (Eq.9).

$$Ni^{2+} + H_2O \rightarrow NiO + 2H^{+} + 2e^{-} \text{(Eq.9)}$$

Electrochemical impedance spectroscopy (EIS) is an important technique for the investigation of the corrosion of metals. EIS provides a non-destructive assessment of the corrosion behaviour. EIS has the advantage that the ohmic drop does not affect the measurement [36].

In Figure 7, we have represented the EIS in the Nyquist plane of the Cu-Ni in tap water, in the absence and the presence of various concentrations of marble powder after 1 hour of immersion in free potential of corrosion.

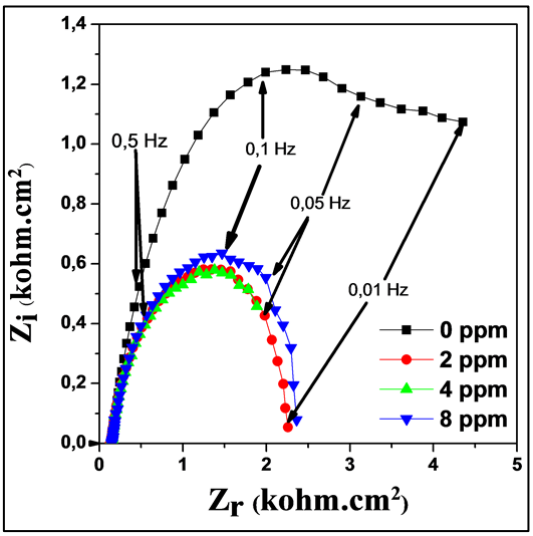


**Figure 7: Nyquist impedance diagrams of Cu-Ni alloy in tap water in the absence and presence of different concentrations of marble powder**

The Nyquist impedance diagram of cupronickel in tap water in the absence of marble water brings up two distinct fields (high and low frequency). At high frequency region, there is a semi circle characterizing a capacitive loop. The semicircles at high frequencies are generally associated with the relaxation of electrical

double-layer capacitors, and the diameters of the high-frequency capacitive loops can be considered as the charge-transfer resistance. This capacitive loop is characterized by a charge transfer resistance ($R_{ct}$=3.6 kΩ) and a double layer capacitor (*CPE*=125 µFcm$^{-2}$). The straight line in the low frequency region could be associated with a diffusional phenomenon (Open Warburg diffusion impedance, $Z_d$=1.32kΩ). The appearance of this phenomenon confirms the formation of a porous surface film consisting of oxides of copper and nickel.

The impedance spectra of copper-nickel in the presence of marble powder are different from those in absence, both in the form and size, reflecting a change in the electrochemical process. The diameter of the capacitive loop increases progressively with increasing the concentration of the powder (Figure 7). Indeed, we observed a slight increase of $R_{ct}$ with marble concentration reaching a maximum for the concentration of 8 ppm.

In the low frequency region, we observed the disappearance of the second scale time probably attributed to a combination of two mechanisms. The first one is related to mechanical corrosion products film removal by hydrodynamic forces [59], the second one is the mechanical abrasion of corrosion products caused by the impact of solid marble particles against the surface. These two phenomena change the corrosion rate by removal of the corrosion layer products and exposing the metal surface to the corrosive medium (electrolyte) [9].

Figure 8 presents the mechanism of Cu-Ni corrosion as function of marble powder concentration.

In the absence of marble powder (Figure 8) and after 1 hour of immersion, the $R_{ct}$ increases. This is caused by the growth of the passive copper oxide film on the alloy surface. However, in the presence of marble powder, the behaviour of the alloy for the three concentrations (Figure 8) is different from that at 0 ppm. A decrease in $R_{ct}$ is observed for the concentration of 2 and 4 ppm whereas an increase of the $R_{ct}$ is clearly recorded for 8 ppm. This latter can be attributed to a mechanical phenomenon; the shock of solid particles of marble together likely causes a reduction of the grain size of marble (compared to 2 and 4 ppm) facilitating their insertion into surface defects by sealing reducing the active sites.

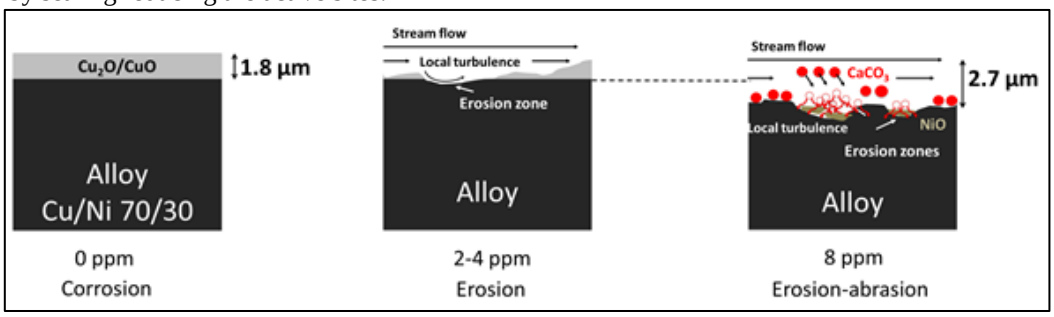


**Figure 8: Schematic process of the alloy Cu-Ni behavior in the tap water in the absence or presence of marble powder**

The analysis of parameters related to electrochemical impedance measurements (Table 7) shows that the $R_{ct}$ decreases, whereas the *CPE* increases in the presence of marble powder compared to that in the absence. In addition, we observed that the average *CPE* remains of the same order of magnitude in the presence of marble powder.

**Table7: Electrochemical impedance parameters of Cu-Ni alloy immersed in tap water in the absence and the presence of different concentrations of marble powder**

| Marble powder concentration (ppm) | $R_e$ (Ω cm²) | CPE (µFcm$^{-2}$) | $R_{ct}$ (kΩcm²) | $Z_d$ (kΩcm²) |
|---|---|---|---|---|
| 0 | 145.5 | 125 | 3.6 | 1.32 |
| 2 | 134 | 188 | 2.152 | 0 |
| 4 | 144 | 198 | 1.978 | 0 |
| 8 | 149.8 | 197 | 2.263 | 0 |

The values of charge transfer resistance $R_{ct}$ are calculated from the difference in impedance at high and low frequencies on the real axis [60]. The value of the double layer capacitor $C_{dl}$ is determined at characteristic of the frequency from the equation:

$$f(-Z_{im_{max}}) = \frac{1}{2\pi C_{dl} R_{ct}} \quad \text{(Eq.10)}$$

In our study, the values obtained for the *CPE* are of the order of 10$^{-4}$ F.cm$^{-2}$. These values reported by different authors [61,62] can be attributed to the response of the electrode relative to the diffusion phenomena (Open Warburg diffusion impedance).

The spectra of EIS were modeled with an equivalent circuit (**Figure 9)** proposing with **"**Zview 6.0" software according to the electrochemical phenomena.

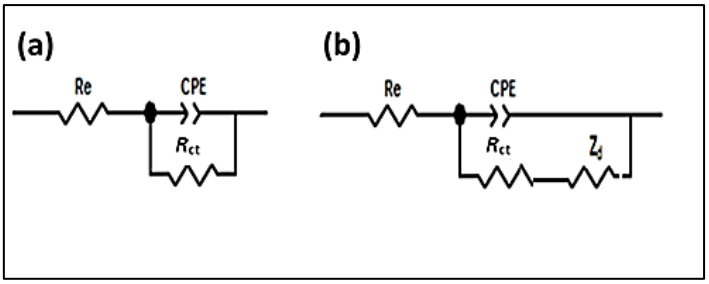


**Figure 9: Equivalent electrical circuit models representing the cupronickel/ electrolyte interface: (a) in the presence of marble powder and (b) in the absence of marble powder**

The physical components shown in the equivalent circuit are:

- $R_e$: The resistance of the medium.
- *CPE*: The phase constant element.
- $R_{ct}$: The charge transfer resistance of the metal / solution.
- $Z_d$: The diffusion impedance.

The impedance of an equivalent circuit of **CPE** can be expressed by either equation [63,64]:

$$Z_{\mathrm{CPE}} = \frac{1}{Q(j\omega)^{\alpha}} \text{(Eq.11)}$$

Where
$Q$ is defined as fitting constant in $\Omega^{-1}m^2s^{\alpha}$,
$\omega$ is the sine wave modulation angular frequency ($rads^{-1}$),
$j^2=-1$ is the imaginary number and $\alpha$is the *CPE* exponent. $A$ is associated with the electrode surface roughness [65]:

$$\alpha = \frac{A}{A_0} \text{(Eq.12)}$$

Where $A$ and $A_0$ are the apparent and real surface area, respectively.

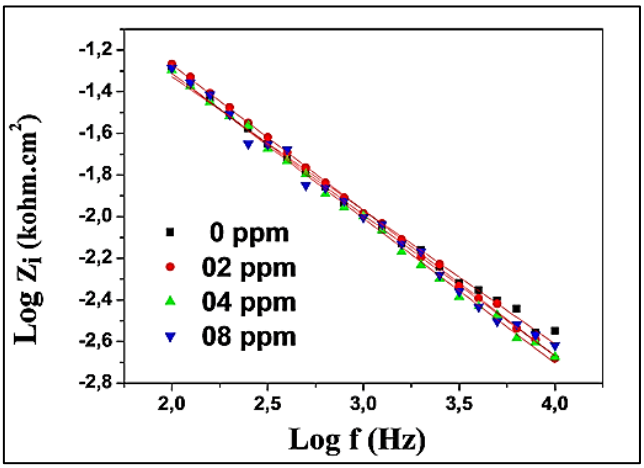


**Figure 10: Imaginary part of the impedance plotted versus the frequency**

In order to justify the presence of a constant phase element (*CPE*) in the equivalent circuit diagram, we plot in Figure10 the logarithm of the imaginary part of the impedance versus the logarithm of the frequency ($\log(|Z_{im}|) = f(\log(f))$ [66,67].
Given that the imaginary part is independent of the electrolyte resistance, the slope determined in the high frequencies domain by linear regression is -0.67, which means that the *CPE* exponent $\alpha = 0.67 \neq 1$ confirming the presence of *CPE* at high frequencies [68].

## CONCLUSION

In summary, it has been shown by electrochemical and structural measurements that the presence of marble powder decreases the corrosion current density of cupronickel. The weight loss measurements showed that the corrosion rate after 30 days of immersion in tap water are 21.6 µm/year in the absence of marble powder and 33.2 µm/year in the presence of 8 ppm of marble.

The structural characterizations by optical and Raman spectroscopy show the formation a friable oxide layer consisting of $Cu_2O$ and CuO in the absence of marble powder in water. In presence of marble particles in water, we revealed the formation of an inhomogeneous oxide layer consisting of both $Cu_2O$, NiO and calcite.
These results are in good agreement with the electrochemical data and thus confirmed the difference in the cupronickel surface composition after 30 days in the presence and absence of marble.
Our study showed the intervention of several phenomena depending on the absence or presence of the marble powder. In the absence of marble powder, we have observed the appearance of the diffusion phenomena (Warburg open), which confirm the formation of a porous surface film.
In the presence of marble powder, we have also observed the disappearance of the diffusion phenomena probably attributed to the combination of two mechanisms: the hydromechanic effect and the mechanical abrasion.
The presence of marble solid particles, in flowing water, lead to damages of the protective film formed on the alloy surface, and a complex phenomenon of erosion and abrasion is evidenced.
Moreover, at 08 ppm of the marble powder, we have clearly shown that the shock of solid particles of marble together likely causes the reduction of the grain size of marble which may facilitate their insertion into surface defects.

## ACKNOWLEDGEMENT

Special thanks to Yassine El Mendili (from CRISMAT/ENSICAEN, UMR CNRS 6508, Université de Caen Basse-Normandie) for the valuable discussions and helpful suggestions.

## REFERENCES

[1] JD De Lassale. Utilisation des marbres, Editions H. Vial, **2005.**
[2] R Malpani; SC Jegarkal ; R Shepur; R Kiran; VK Adi. *Int J Innov Tech Expl Eng*, **2014**, 4, 39-42.
[3] NM Soliman. *Int J Current Eng Tech*, **2013,** 3, 1863-1870.
[4] GC Ulubeyli; R Artir. *Procedia-Soc Behav Sci*, **2015,** 195, 2181-2190.
[5] D Singh; MA Khan; A Kumar. *Int Res J Eng Tech*, **2016,** 3(3), 524-526.
[6] N Herz; M Waelkens. *Brill Archive*, **1988**.
[7] B Demirel. *Int J Phys Sci*, **2010,** 5(9), 1372-1380.
[8] A Zaki. *Br Corros J*, **2001,** 36(1), 59-64.
[9] RF North; MJ Pryor. *J Corros Sci*, **1970,** 10, 297-311.
[10] M Metikoš-Huković; RBI Rončević; Z Grubač. Desalination, **2011,** 276, 228-232.
[11] HG Bachmann. The identification of slags from archaeological sites. published by the Institute of Archaeology of London, Occasional Publication No. 6, Institute of Archaeology, London, **1982.**
[12] L Babouri; K Belmokre; A Kabir; A Abdelouas; Y El Mendili. *J Chem Pharm Res***, 2015,** 7(4), 1175-1186.
[13] BJ Little; JS Lee. Wiley Inter Sci., A John Wiley& Sons, Inc., Publication, **2007.**
[14] W Schleich. Corrosion, Paper No 5222, Houston, **2005.**
[15] http,//www.belgaqua.be/homeEng.htm
[16] BC Syrett. Sulfide attack in stearn surface condensers. Conf. on environmental degradation of engineering materials in an agressive environment, Virginia Polytechnic Institute, **1981.**
[17] AM Beccaria; G Poggi; P Traverso. *Corros Sci*, **1991,** 32(11), 1263-1275.
[18] JN AL-Hajii; MR Reda. *Corros Sci*,**1993,** 34(1), 163-177.
[19] DR Lenard; RR Welland. *Corrosion*, **1998,** 599.
[20] DR Lenard. Corrosion, **2002,** 02185.
[21] A Klassert; L Tikana. *Euro Corr*, **2004**.
[22] RM Kain; BE Webber. *Corrosion*, **1997,** 422.
[23] OM Aylor; RA Hays; RM Kain. *Corrosion*, **1999,** 329.
[24] H Hoffmeister; J Ulllrich. *Corrosion*, **2000.**
[25] DD Macdonald; BC Syrett; SS Wing. *Corrosion*, **1979,** 35(8), 367-378.
[26] DD Macdonald; BC Syrett; SS Wing. Annual Report of Naval Research, ONR, **1979,** 36-116.
[27] B Trachli. Phd Thesis, P&M Curie University–Kénitra University, Paris–Kénitra, **2001**.
[28] R Francis. *Br Corros J*, **1985,** 20(4), 167-173.
[29] DA Jones. Principles and Prevention of Corrosion. Maxwell Macmillan Pub, New York, **1992**.
[30] MS Parvisi; A Aladjem; JE Castle. *Int Mater Rev*, **1988**, 33(4), 169-200.
[31] KD Efird. *Mater Perform.*, **1976,** 15(4), 16-25.
[32] JL Heuze; B Dubois. *J Phys Colloques*, **1988,** 49, C3-339-C3-346.
[33] H Isaacs H; M Kendig. *Corrosion*, **1980,** 36(6), 269-274.

[34] Y El Mendili; A Abdelouas; H El Hajj; JF Bardeau. *RSC Advances*, **2013,** 3(48), 26343-26351.
[35] Y El Mendili; AAbdelouas; A AïtChaou; JF Bardeau; ML Schlegel. *Corros Sci*, **2014,** 88, 56-65.
[36] L Babouri; K Belmokre; Y Mendili; A Abdelouas; JF Bardeau. *Int J Electrochem Sci*, **2015,** 10, 7818-7839.
[37] M Prencipe; F Pascale; C Zicovich-Wilson; V Saunders; R Orlando; R Dovesi. *Phys Chem Miner*, **2004,** 31, 559-564.
[38] T Beuvier; JF Bardeau; B Calvignac; G Corbel; F Hindre; JM Greneche; F Boury; A Gibaud. *J Raman Spectroscopy*, **2013,** 44(3), 489-495.
[39] WD Bischoff; SK Sharma; FT Mackenzie. *Am.Mineral*, **1985,** 70, 581-589.
[40] PF McMillan; AM Hofmeister. In Hawthorne F. C. (ed), Washington, Reviews in Mineralogy, **1988,** 18, 99-159
[41] M De La Pierre; C Carteret; L Maschio; E André; R Orlando; R Dovesi. *J Chem Phys*, **2014,** 140(16), 164509
[42] K Huang. *Z Physik*, **1963,** 171, 213-225.
[43] P Dawson; MM Hargreave; GR Wilkinson. *J Phys Chem Solids*, **1973,** 34, 2201-2208.
[44] A Compaan. *Solid State Commun*, **1975,** 16, 293-296.
[45] D Powell; A Compaan; JR Macdonald; RA Forman. *Phys Rev*, **1975,** B12, 20-25.
[46] M Balkanski; MA Nusimovici; J Reydellet. *Solid State Commun*, **1969,** 7, 815-818.
[47] S Åsbrink; LJ Norrby. *Acta Crystallogr Sect*, **1970,** B26, 8-15.
[48] RWG Wyckoff. Crystal Structures, 2nd edition, International Science Publishers, New York, **1963.**
[49] G Kliche; ZV Popovic. *Phys Rev*, **1990,** B 42, 10060-10066
[50] T Yu; X Zhao; ZX Shen; YH Wu; WH Su. *J Crystal Growth*, **2004,** 268, 590-595.
[51] SH Lee; HM Cheong; NG Park; CE Tracy; A Mascarenhas; DK Benson; SK Deb. *Solid State Ionics*, **2001,** 14, 135-139.
[52] KW Nam; KB Kim. *Electrochem Soc*, **2002,** 149(3), A346-A354.
[53] S Sauvé; MB McBride;WA Norvell; WH Hendershot. *Water Air Soil Pollution*, **1997**, 100, 133-149.
[54] Y LiL; RS Li. *Can Geotech*, **2000**, 37:267-307.
[55] HH Strehblow; B Titze. *Electrochimica Acta*, **1980**, 25, 839-850.
[56] JC Hamilton; JC Farmer; RJ Anderson. *J Electrochem Soc*, **1986,** 133, 739-745.
[57] Y Van Ingelgem; E Tourwé; J Vereecken; A Hubin. *Electrochimica Acta*, **2008,** 53, 7523-7530.
[58] KP Fitz Gerald; J Nairn; G Skennerton; A Atrens. *Corros Sci*, **2006,** 48, 2480-2509.
[59] RW Revie. Electro-chemical Society Series. ed., Uhlig's Corrosion Handbook, 2nd edition, New York, NY, John Wiley and Sons, Inc., **2000,** 249-272.
[60] T Tsuru; S Haruyama; B Gijustu. *J Japan Soc Corros Eng*, **1978,** 27, 573-581.
[61] EJL Schouler; N Mesbahi; G Vitter. *Solid State Ionics*, **1983**, 9-10, 989-996.
[62] E Boehm. Phd Thesis, Université Bordeaux 1, France, **2002.**
[63] GJ Brug; E Van Den; ALG Eden; M Sluyters-Rehbach; JH Sluyters. *J Electroanal Chem*, **1984,** 176, 275-295.
[64] MA Elmorsi; AM Hassanein. *Corros Sci*, **1999,** 41, 2337-2374.
[65] F Ammeloot; C Fiaud, EMM Sutter. *Electrochim Acta*, **1997,** 43:3565-3574.
[66] ME Orazem, N Pébère, B Tribollet, PV 2004-14 Electrochemical Society, Pennington, New Jersey, **2005.**
[67] ME Orazem; N Pébère; B Tribollet. *J Electrochem Soc*, **2006,** 153(4), B129-B136.
[68] O Devos; C.Gabrieli; B Tribollet. *Electrochimica Acta*, **2006**, 51, 1413-1422.